Compartmental Model for Epidemics with Contact Tracing and Isolation under Arbitrary Degree Distribution

Elan Ocheretner [1], Amir Leshem[1*]

[1]Faculty of Engineering, Bar-Ilan University, Ramat Gan, Israel

[*]Corresponding author: Amir Leshem; E-mail: amir.leshem@biu.ac.il.

Abstract

The recent COVID-19 epidemic demonstrated the need and importance of epidemic models as a tool for policy-making during times of uncertainty, allowing the decision-makers to test different intervention techniques and scenarios. Furthermore, tools such as large-scale contact tracing became technologically feasible for the first time. While large-scale agent-based simulations are nowadays part of the toolboxes, good analytical models allow for much faster testing of scenarios. Unfortunately, good models that consider contact tracing and quarantine, and allow for different degree distributions do not exist. To overcome these shortcomings of existing models we propose a new simple compartmental model that integrates quarantine and contact tracing into the SIR compartmental models with arbitrary degree distribution of nodes to better understand the dynamics of the disease under various parameters of intervention and contagion. Consequently, we analytically derive the epidemic threshold as a function of the degree distribution and the model parameters when both quarantine and contact tracing are used. Simulation results demonstrate and quantify the benefits of quarantine and contact tracing and show the effectiveness of such measures over a large range of epidemic parameters.

Introduction

The outbreak of COVID-19 affected people around the world and provided health, social, and economic challenges [1]. Estimating the impact of the disease [2, 3] and use of mitigation measures [4, 5] can help shape the effect on the population and combat the outbreak.

Epidemiology is the field of science for mathematical modeling for such problems [6, 7]. When researching the field of epidemiology, we can see two distinct approaches: agent-based simulation [8, 9] and compartment modeling [10–12]. The advantage of agent-based simulation is that you can tailor the epidemic to a specific case by simulating different disease parameters on a certain population on the individual level. However, there is a severe limitation with the agent-based simulations. This approach is computationally expensive and time-consuming, as discussed in [13]. This makes it difficult to conclude anything general regarding the epidemic in a given population without simulating the model for many repetitions. The compartmental approach proposes compartmentalizing the population in different states and devising ordinary differential equations to describe at what rate individuals travel between different compartments [14]. The compartment models offer an easy, computationally inexpensive way to model the propagation of the disease and provide insight for future scenarios, allowing quick decision-making.

The most popular compartmental model is the SIR model, it divides the population into three models S—susceptible, I—infected, and R—recovered. Examples of other models include SIS (susceptible—infected-susceptible) [15] where infected individuals become susceptible again after some time, SIRQ (susceptible—infected—recovered—quarantined) [16] which incorporates quarantine of infectious individuals. Usually, when such models are used, it is assumed the population is a well-mixed one. The issue with such an assumption is that it doesn't describe reality [17]. To resolve this a degree-based approach is used [18, 19], and it assumes that vertices with the same degree behave similarly, in [12] we see that this approximation is a good one. [20–22] solve the case of the SIR model with degree distribution, where [22] specifically explores the subject on a more complex network.

In the recent COVID-19, we saw that implementing contact tracing and isolation techniques could be used to control the outbreak [23], [24], [25], [26], [27], [28], that is why in our research, we focused on incorporating quarantine and contact tracing into the classic SIR compartmental model under any arbitrary degree distribution. This grows more relevant in time as improve-

ments in technology can help make contact tracing easier [29]. Some papers try to solve this problem in the agent-based approach [30], [31], [27], while others used compartment models but only using fully-mixed models [32], [33]. Our model enriches the SIR model by changing S, and I's compartments to two compartments each (Not quarantined and quarantined states for each previous state) and add additional transitions between states. Papers [30], [34], [32], [33] are closest to our model. The model in [33] is fully mixed and does not address any social networks. [30] quantifies the network effects of contact tracing using configuration models, but doesn't provide the equations of the model for further research. In addition, [30] and [34] assume a different tracing process – the tracing occurs immediately as an infected individual enters quarantine. The rate of contact tracing differs in several methods of tracing, as can be seen in [29], also the delay highly affects the impact of contact tracing [35]. In our model, we assume there is a delay to contact tracing similar to [32]. In our research, we simplify and provide easier equations to work with than in [32]. We devise a simple, equation-based way to quantify the effect of contact tracing and isolation on epidemic spread. For the case of a regular graph, we provide an analytical solution to reduce the equations to a single equation to solve to further simplify the calculation. In addition, we show that the regular graph case is similar to Erdős–Rényi. This important result means that any degree distribution that can be approximated as Erdős–Rényi and only one equation needs to be solved. Moreover, we can clearly see in the results the validity of our model and the effectiveness of tracing and quarantine measures over a large range of epidemic parameters. In the future, our model can be a foundation for other models incorporating any additional measures of epidemic control.

Results

In this paper, we extend the classical SIR models with arbitrary degree distribution [12], [18,19], to the case where quarantine and contact tracing are available measures to limit the spread of the epidemic. These measures have been widely applied during the recent pandemic [36–39], however, we were unable to find simple compartmental models incorporating these measures. Our main results include the development of the compartmental model incorporating both quarantine and contact tracing, for an arbitrary degree distribution model. The model is depicted in Fig. 1. For this model, we derive a simple closed-form formula for the epidemic threshold.

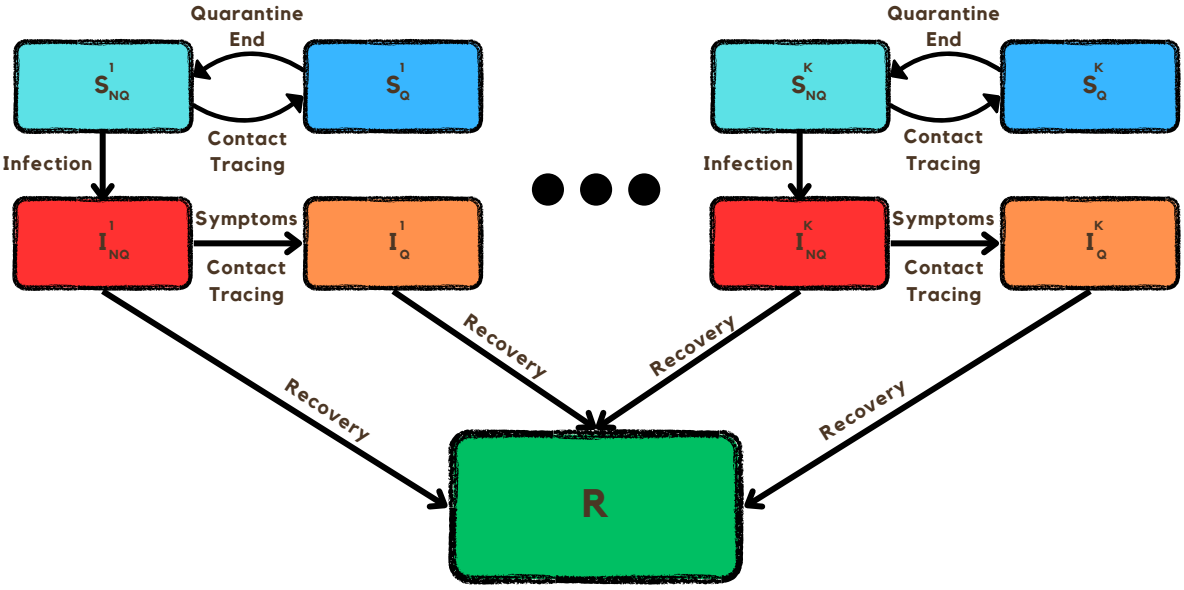

Fig. 1: An illustration of the SIRCQ model proposed in this paper. For each degree k, we have four possible compartments $(S^k_{NQ}, S^k_Q, I^k_{NQ}, I^k_Q)$, whereas the recovered compartment *R* is for all degrees.

Then we significantly simplify the equations in the case of a contact graph with a fixed degree of all nodes. This generalizes the classical SIR model, where each node can be connected to all other nodes. We show, by simulations, that this simplification provides an excellent approximation for the Erdős–Rényi family of random graphs [40], [41].

To validate our theoretical results, we performed extensive comparisons with agent-based models for both scale-free degree graphs and regular graphs. First, we compared the temporal epidemic evolution, and then we evaluated the proportion of infected people under various model parameters. We also validate the formula for the epidemic threshold in both cases. The results show good agreements between theory and simulation and validate our results.

SIRCQ model

We begin with a detailed description of the proposed model. Note that the interplay between contact tracing and quarantine is complex and is further complicated by the stochastic nature of contact tracing and the variability in symptom onset. Our model aims to capture these dynamics to provide insights into the effectiveness of quarantine and contact tracing as strategies to control the spread of infectious diseases. The model takes the classical SIR compartmental model with degree distribution and splits each susceptible (S^k) and infected (I^k) compartment into two compartments each, one with quarantined individuals and another with non-quarantined individuals. In total, we have five distinct compartments for each degree in the contact graph: susceptible individuals who are quarantined (S^k_Q), susceptible individuals who are not quarantined (S^k_{NQ}), infected individuals who are quarantined (I^k_Q), infected individuals not quarantined (I^k_{NQ}), and recovered individuals (R). Fig. 1 depicts the transitions between compartments.

While transitions are made between compartments of each degree, the transition rate is determined by the cumulative amount of infected individuals in all infected compartments. The dynamics of the model are governed by a set of differential equations that account for the arbitrary degree distribution of the contact network, representing the heterogeneity in the number of contacts per individual. For each degree k, there are five equations corresponding to the five compartments. These equations represent the net inflow of individuals to the corresponding compartment and are coupled through the total number of infected individuals.

We will start describing the transitions in the compartments with the infection process, which moves individuals from S^k_{NQ} to I^k_{NQ}. Newman [12] presents the Susceptible — Infectious — Recovered (SIR) model with degree-based distribution. The excess degree distribution is used in order to describe the infection process. We will use a similar process for our model. The reason excess degree distribution is used is that a susceptible vertex (A) can be infected by an infected neighbor (B) only if B has another infected neighbor (C) who is not susceptible. Thus, to get the infection probability we need to consider the excess degree distribution of B, so that we don't include A. In short, the infection rate of each susceptible individual depends on 3 parameters: the probability of infection upon contact, the degree of the individual, and the probability that their contact/neighbor is infected, which as we mentioned above is determined by the excess degree of the contact.

Symptomatic transfer to quarantine is another feature of our model, where individuals in the

I^k_{NQ} compartment are moved to the corresponding I^k_Q compartment based on the onset of symptoms. This process considers the delay between infection and the onset of symptoms, which plays a significant role in the disease dynamics. In our model, symptoms are assumed to follow a geometrical probability distribution over the course of the infection. This process considers the delay between infection and the onset of symptoms, which plays a significant role in the disease dynamics.

Contact tracing is modeled as a mechanism that transitions individuals from the S^k_{NQ} to the corresponding S^k_Q compartment, and from the I^k_{NQ} to the corresponding I^k_Q compartment, upon identification of their contact with a *known* infected individual, which means the traced individual has to be from IQ. The efficiency of the contact tracing process is a critical parameter, influencing the rate at which individuals are quarantined and thereby affecting the spread of the infection. We parameterize the efficiency of contact tracing as the rate of contact tracing, which is assumed to follow a geometrical probability distribution from the time an individual enters the I^k_Q compartment. This can represent different contact-tracing mechanisms, such as electronic contact tracing and epidemiological investigations [29, 35]. Similarly to infection, contact tracing is affected by the excess degree distribution (which is a function of all infected compartments) as the infected and quarantined individuals had to be traced from another neighbor, who is in quarantine, and is not necessarily of the same degree.

The recovery process is modeled through a transition from both IQ and INQ compartments to the R compartment, using a geometrical probability distribution similar to the symptoms' onset. The recovery signifies the development of immunity or the end of the infectious period.

The combination of all this information is depicted in Fig. 1, we can see all the compartments for each degree and all the possible transitions mentioned above. This model provides a quick and valuable tool for public health officials and policymakers to evaluate the implications of different intervention strategies, offering a more nuanced understanding of epidemic control in the face of uncertainty and incomplete information. The implications of our findings are particularly relevant for the strategic design of measures to mitigate the spread of future epidemics. Detailed derivation of these equations is given in the methods section.

Epidemic threshold of SIRCQ model

Our main theoretical result is the computation of the epidemic threshold for the SIRCQ model in two cases: Arbitrary degree distribution and for the special case of a regular graph. The computation utilizes the technique of [42] by defining the next-generation transmission and transition matrices to calculate R_0. For arbitrary degree distribution, the epidemic threshold is growing linearly with the infection parameter and the mean degree of a neighbor, also known as the mean excess degree and inversely proportional to the sum of the inverse of the mean time for the appearance of symptoms and the recovery rate. The detailed calculation is given in the Methods section under "Calculation of the epidemic threshold for arbitrary degree distribution".

The mean degree of a neighbor is the important parameter, similar to [12] for the degree-based SIR. As is expected, contact tracing does not affect the epidemic threshold, but rather reduces the spreading rate when the epidemic evolves. The logic behind it is that when everyone is virtually susceptible and there are no infected people in quarantine, contact tracing is not yet effective and does not determine the disease outbreak. We also provide a simpler derivation for the case of a k-regular graph. This generalizes the standard SIR case by limiting the number of contacts of each person to a specific number.

Comparison of the compartment model and agent-based model

To validate our model we compare the numerical solution of the compartmental model equations with an agent-based model (ABM). The results show good agreement between the models, which verifies our equations. Fig. 2 compares the temporal behavior of the two models for power law distributed degrees of the nodes. The minimal degree was 8 and the mean degree was 40. This generates a highly heterogeneous degree distribution. The disease parameters are determined by the mean transition time between compartments that are geometrically distributed. The probability of infection per contact (β) was selected to be 0.02, the recovery rate (γ) was chosen to be 0.14 (7 days), the contact tracing rate (p_{ct}) was selected to be 0.5 (2 days), the rate of return of susceptible individuals from quarantine (θ_s) was chosen to be 0.07 (14 days), and the rate of symptoms appearance ($p_{symptoms}$) was selected to be 0.25 (4 days).

Fig. 2a shows the relative population of the susceptible compartment as a function of time in Newman's model (no quarantine and no contact tracing), The reproduction number in this case is $R_0 \approx 40$. If we add the symptoms' onset and contact tracing we get Fig. 2b. We can clearly

see different behavior in the susceptible population, the proportion of infected people in the population after the epidemic ends (r_∞) is lowered from 0.86 to 0.012. This directly expresses the power of quarantine and contact tracing, showing how important these measures are.

Fig. 2c and Fig. 2d show the relative infected population as a function of time. In all the results in Fig. 2 we can see a clear agreement between the results of the agent-based and compartmental models. The compartmental model is close to the median of the agent-based model and falls well within the $10\% - 90\%$ confidence interval.

Similarly, Fig. 3 presents the same results for regular graphs. In this case, there is also a clear agreement between the results of the agent-based and compartmental models. This further enhances the validity of our results by showing that the compartmental model agrees with the agent-based model for two significantly different degree distributions.

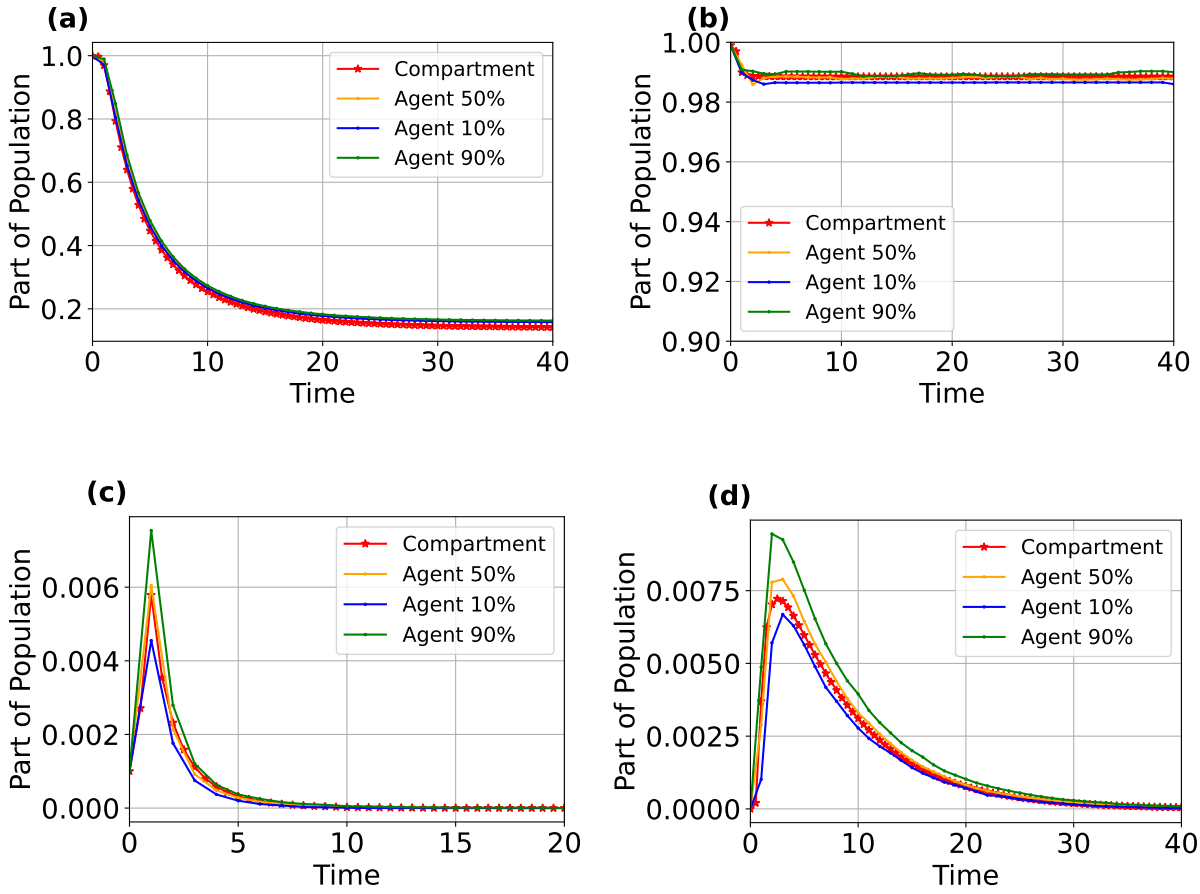

Fig. 2: Comparison of the compartment model and agent-based model in the power law case. The sub-figures are susceptible in Newman's model (a) susceptible in the SIRCQ model (b), infected and non-quarantined (c), and infected and quarantined (d). The range is between 0 and 1 because we normalize by the population. The parameters of the epidemic are: $\beta = 0.02$, $\gamma = 0.14$, $p_{ct} = 0.5$, $\theta_s = 0.07$, $p_{symptoms} = 0.25$. For (d) symptoms and contact tracing are zero ($p_{ct} = 0$, $p_{symptoms} = 0$).

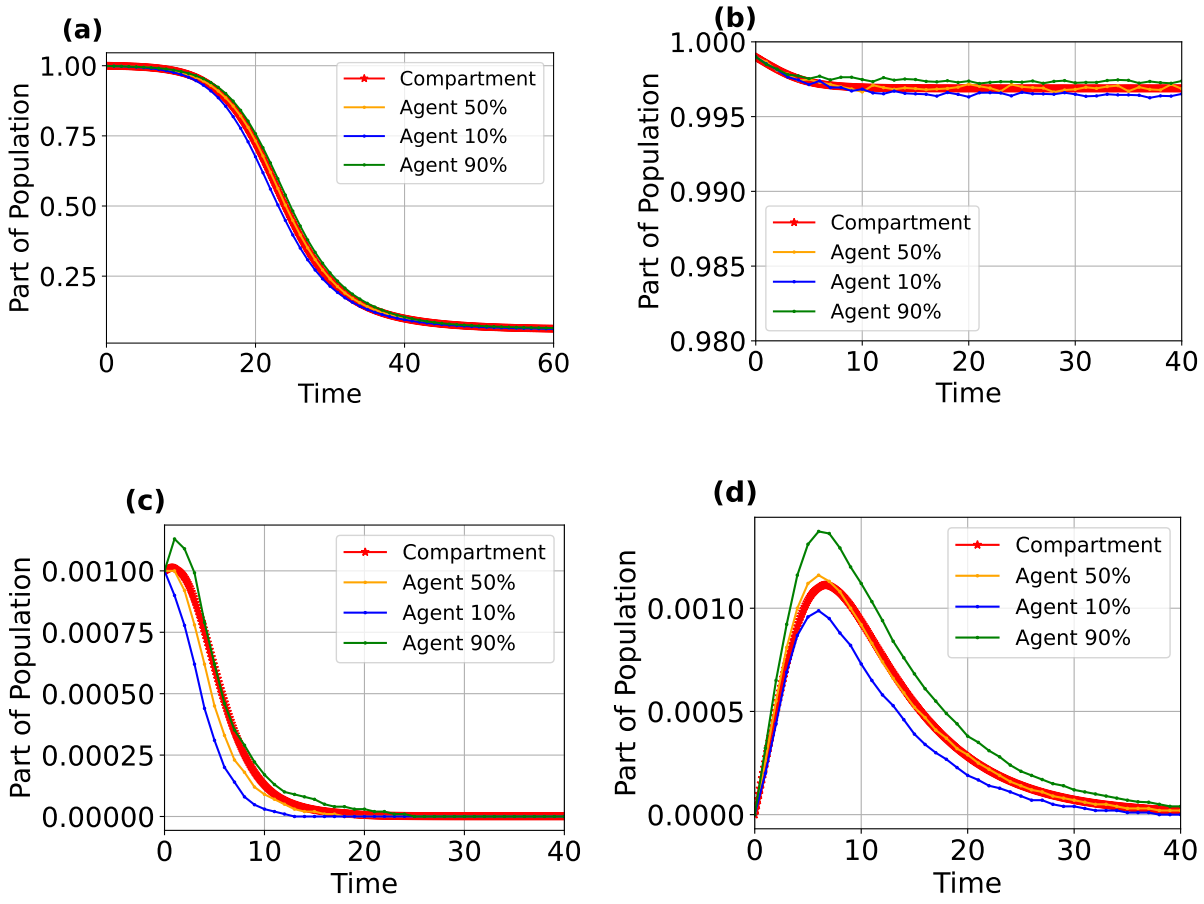

Fig. 3: Comparison of the compartment model and agent-based model in the regular-graph case. The sub-figures are susceptible in Newman's model (a) total susceptible in the SIRCQ model (b), infected and non-quarantined (c), and infected and quarantined (d). The range is between 0 and 1 because we normalize by the population. The parameters of the epidemic are: $\beta = 0.002$, $\gamma = 0.14$, $p_{ct} = 0.5$, $\theta_s = 0.07$, $p_{symptoms} = 0.25$. For (d) symptoms and contact tracing are zero ($p_{ct} = 0$, $p_{symptoms} = 0$). The degree was chosen to be 281, the same as the mean excess degree in the power-law case.

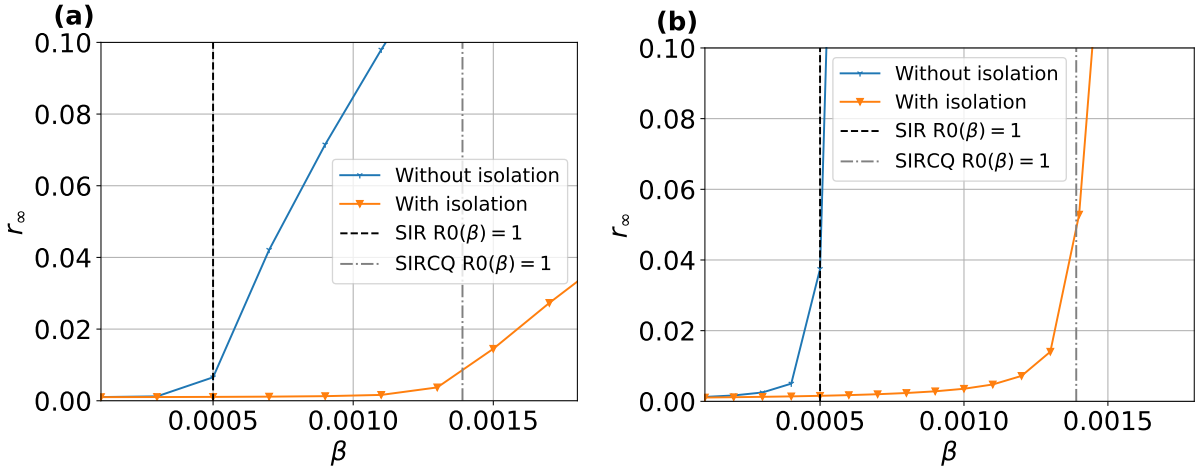

Fig. 4: Epidemic threshold expressed with r_∞ as a function of β in a power law degree distribution(a) and regular-graph degree distribution(b).

Experimental validation of the formula for R_0

The next result validates our theoretical computation of the epidemic threshold. We compare the computed epidemic threshold and the numerical results of the compartmental model. Fig. 4 depicts r_∞ versus the infection parameter (β) for power law and regular graphs, respectively, with all other epidemic parameters constant in different scenarios. We observe a good agreement between the theoretical epidemic threshold and the beginning of an exponential growth of the total number of infected people as a function of the infection parameter. In Fig. 4a, since the excess degree is 281, $R_0 = 1$ for $\beta \approx 0.0014$ when quarantine is used and $\beta \approx 0.0005$ without quarantine. For the regular graph result, we chose the degree to be the same as the excess degree of the power law graph to have the same thresholds. We can see this result in Fig. 4b.

The effects of contact tracing and isolation on the number of infected cases in the population

Our next result studies the impact of contact tracing on the total infected population. We show that accelerating the contact tracing can significantly reduce the total number of infected people. Fig. 5 and Fig. 6 present different scenarios for power law and regular graphs, respectively. Fig. 5a and Fig. 6a show the SIR model with the same degree distribution but without quarantine or contact tracing [43] where there are only three compartments. The range of the infection parameter β was selected such that r_∞ covers the interval from 0 to 0.95 in this model. We used the same infection parameters with various contact tracing and quarantine parameters to evaluate the gain of contact tracing and quarantine as compared to this model. Figures 5b and 6b present a different scenario for symptoms-based quarantine only, we can see a significant reduction in the total infection population by up to 30% for the highest probability of infection. The remaining sub-figures consider the effect of adding contact tracing on top of symptoms-based quarantine. We can see a significant reduction in the total infected population, further improving upon the symptoms-based quarantine. In addition, in every scenario, there is a good agreement between the ABM and the compartment model, further validating our model. An important advantage of the compartmental model is that the calculation of these results is 3 orders of magnitude faster compared to the ABM model.

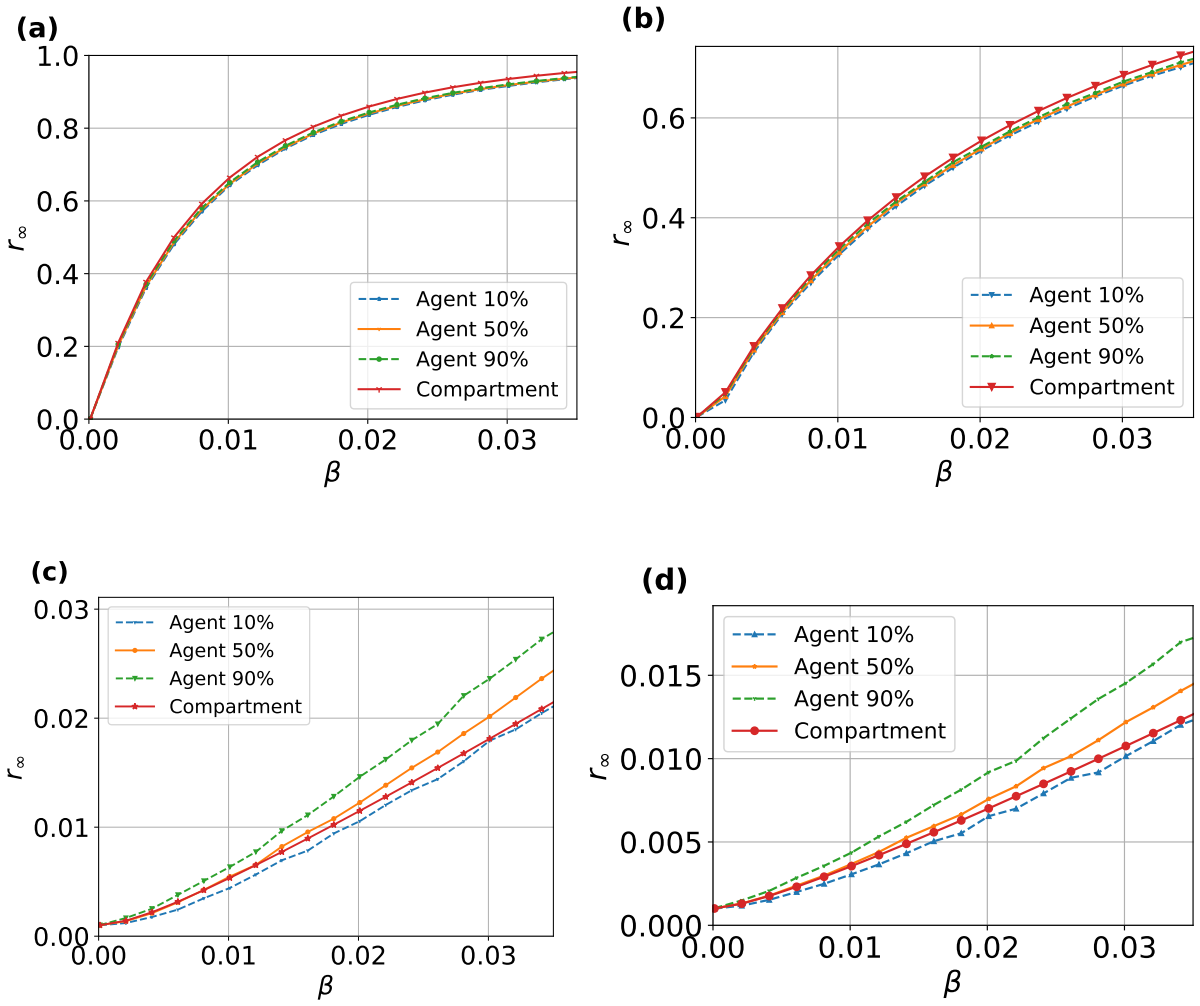

Fig. 5: Comparison of r_∞ as a function of β between agent and compartment in a power law degree distribution. There are 4 sub-figures for different scenarios. Fig. (a) is for No quarantine and no tracing (SIR model with degree distribution), Fig. (b) is for symptom-based quarantine only ($p_{ct} = 0$), Fig. (c) is for quarantine and tracing of $p_{ct} = 0.5$, Fig. (d) is for quarantine and tracing of $p_{ct} = 0.9$.

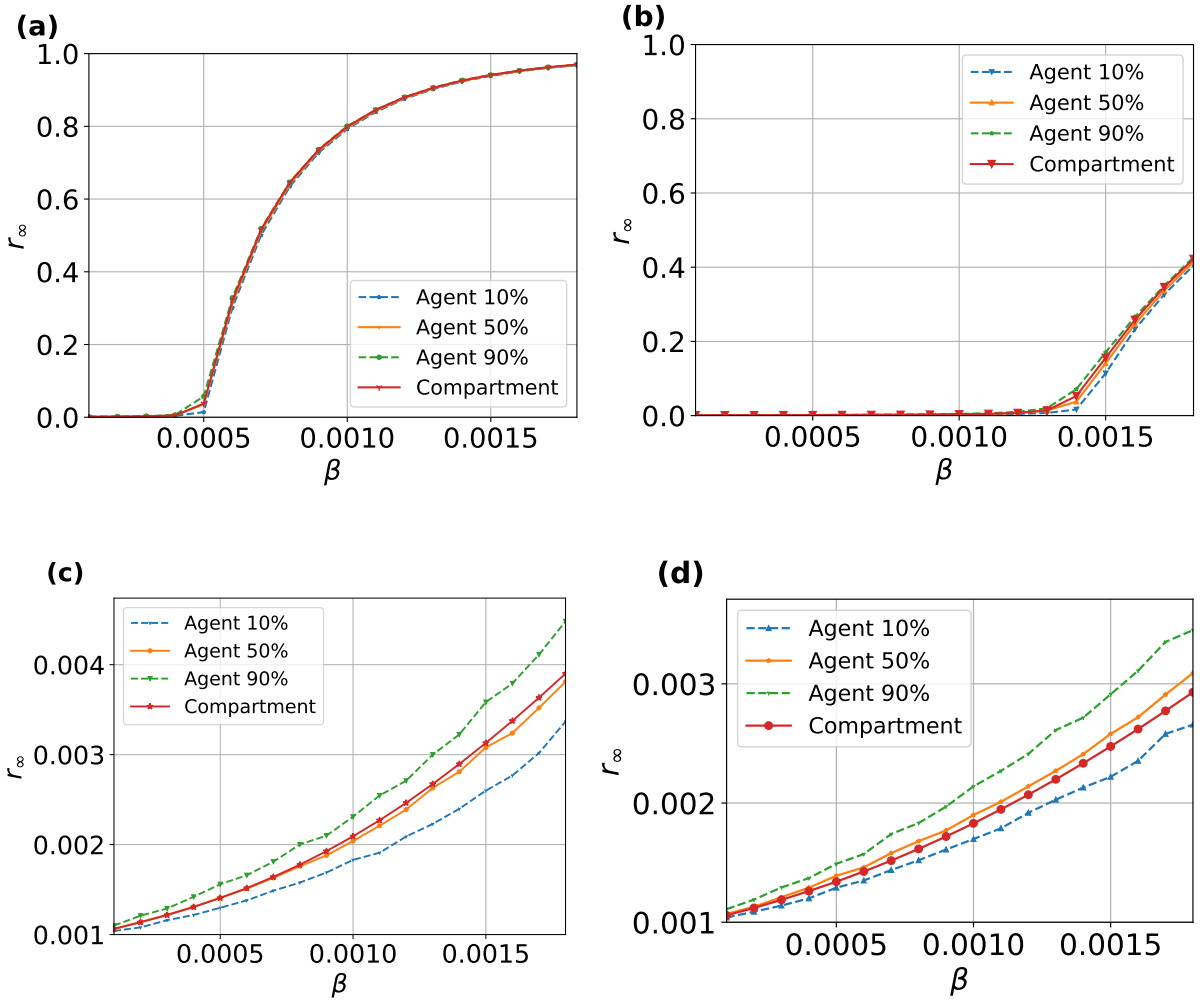

Fig. 6: Comparison of r_∞ as a function of β between agent and compartment in a regular-graph degree distribution. There are 4 traces for different scenarios. Fig. (a) is for No quarantine and no tracing (SIR model with degree distribution), Fig. (b) is for symptom-based quarantine only ($p_{ct} = 0$), Fig. (c) is for quarantine and tracing of $p_{ct} = 0.5$, Fig. (d) is for quarantine and tracing of $p_{ct} = 0.9$. The degree of the graph is 281, as the mean excess degree of the power-law case.

Comparison between Erdős–Rényi and regular graphs

The differences in the epidemic dynamics between the regular graph and the power law graph are significant. Intuitively, regular graphs represent a case where the variation of the degrees is small. This suggests that the results for regular graphs should be a good approximation to the family of Erdős-Renyi graphs. Our final result is the comparison between Erdős–Rényi and regular graphs. Indeed the results show good agreement over a wide range of parameters. This result is very important because it means that our simplification of the regular graph to a single equation is valid for a wide range of degree distributions which include the Erdős–Rényi graphs. Any degree distribution that can be represented as an Erdős–Rényi graph (or even families where the degree distribution is relatively concentrated) can have a simple approximate solution by numerically solving a single equation with a closed form algebraic solution for the other equations instead of solving numerically $5\times K$ equations where K is the number of different degrees of nodes. This result is not surprising, as Erdős–Rényi has a rather small variance and is concentrated around the mean. The degree of the regular graph was chosen as the mean of the Erdős–Rényi degree distribution so that we have Erdős–Rényi with n as the population size and $p = k/n$ where k is the degree of the k-regular graph. In Fig. 7 we see the results, we can see that both the agent-based and the compartmental models of Erdős–Rényi are approximately equal to the k-regular graph results.

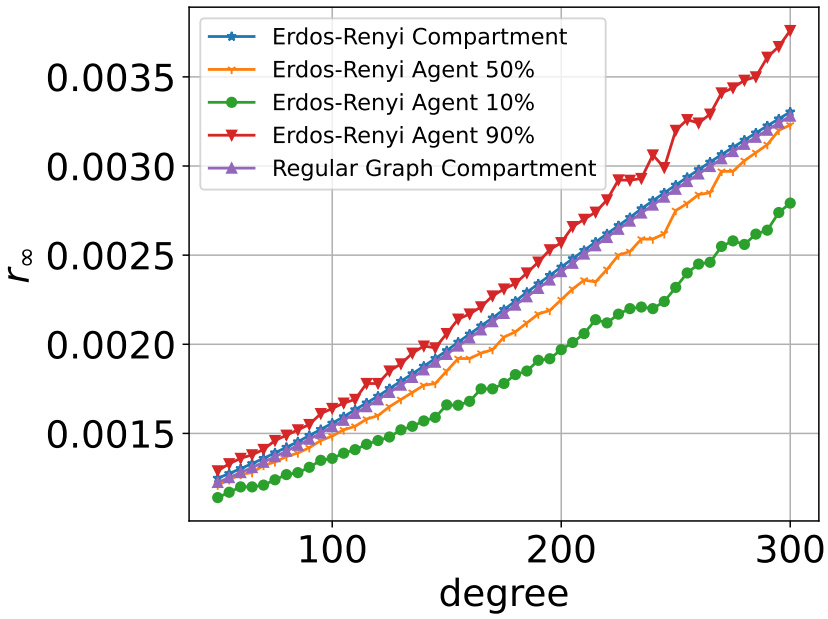

Fig. 7: Comparison of r_∞ as a function of degree between Erdős–Rényi and regular graph degree distributions. We have four traces of Erdős–Rényi, three of which are agent-based simulations and one is compartment-based. We can clearly see that the compartment solution of Erdős–Rényi agrees with the agent-based solution and that the Erdős–Rényi compartment solution is almost identical to the regular graph compartment solution. We chose $\beta = 0.0015$ to make sure $R_0 > 1$ for all degrees in the range.

Discussion

We introduced a novel compartmental model that includes contact tracing and quarantine under an arbitrary degree distribution. We calculated the epidemic threshold in the general case as well as for regular graphs. Moreover, we developed a way to reduce the complexity of the solution for regular graphs to the numerical solution of a single equation. This model allows a much faster evaluation of the impact of contact tracing and quarantine under various models. Since the solution is 3-4 orders of magnitude faster than the ABM even for populations up to 100,000, the acceleration would be more significant when we try to evaluate the impact of the measures on a state level. Hence, the model provides an important tool for policy making and testing various measures under different situations. It also allows quick sensitivity analysis to the various parameters, something that is much harder with agent-based models, and is important when epidemic parameters are noisy estimates derived from real-time epidemic progression. Furthermore, deriving a simple formula for the epidemic threshold provides an even faster means of estimating the impact of quarantine and contact tracing.

We demonstrated the clear impact of contact tracing on epidemic evolution. Isolation slows the spread of the disease and contact tracing significantly enhances that effect. As a result r_∞ drops.

In addition, we showed that the regular graph case has a good agreement with Erdős–Rényi graphs, which can be used for an entire family of degree distributions. We can further generalize this to a larger family of degree distributions, where the degree variation is small. For example, degree distributions that can be approximated by a two-degree model can be represented by 10 differential equations.

In the future, this model can be a foundation for more complex models, as this model introduces a simple way to incorporate contact tracing into compartmental models.

Methods

SIRCQ model development

We now derive the SIRCQ model equations. For each degree, the standard compartments are used for non-quarantined people with degree k and denoted by S^k_{NQ}, I^k_{NQ}. For each degree k we

add two new compartments for people in quarantine. One for susceptible and quarantined (S_Q^k) and the other for infected and quarantined I_Q^k. We note that susceptible and quarantined move back to the susceptible and non-quarantined after a certain time, while infected and quarantined move to the recovered compartment (R). Each of these transitions has its own rate. The model is depicted in Fig. 1.

To describe the model, we use the following notation: p_k is the probability that a vertex has degree k, q_k that the *excess* degree is k, x^k is the part of the population in the compartment x, where x is one of the super compartments (i.e, including all degrees) (s_{nq} - susceptible and not quarantined, s_q - susceptible and quarantined, i_{nq} - infected and not quarantined, i_q - infected and quarantined, r - recovered), normalized by the population size of degree k. For example, s_{nq}^5 is the proportion of susceptible and not quarantined individuals with degree 5 out of all degree 5 population. β is the probability of infection per contact, γ is the recovery rate, v is the probability that a neighbor vertex is infected and not quarantined (regardless of its degree), $\hat{v}$ is the probability that a neighbor vertex is infected and quarantined, p_{ct} is the contact-tracing rate, $p_{symptoms}$ is the symptoms appearance rate, and θ_s is the rate of exiting quarantine.

The equations for the model are:

$$\frac{ds_{nq}^k}{dt} = -\beta k v s_{nq}^k - p_{ct} k \hat{v} s_{nq}^k + \theta_s s_q^k, \tag{1}$$

$$\frac{ds_q^k}{dt} = p_{ct} k \hat{v} s_{nq}^k - \theta_s s_q^k, \tag{2}$$

$$\frac{di_{nq}^k}{dt} = \beta k v s_{nq}^k - p_{ct} k \hat{v} i_{nq}^k - p_{symptoms} i_{nq}^k - \gamma i_{nq}^k, \tag{3}$$

$$\frac{di_q^k}{dt} = p_{ct} k \hat{v} i_{nq}^k + p_{symptoms} i_{nq}^k - \gamma i_q^k, \tag{4}$$

$$\frac{dr^k}{dt} = \gamma (i_{nq}^k + i_q^k). \tag{5}$$

We will now derive these equations similarly to the model of [43]. We begin with the derivation of [12] and modify it to include the new compartments. The equations in [12] are expressed using only $3K$ compartments (s_k - susceptible, i_k - infected, r_k - recovered). Using the notations above the equations in [12] are defined as follows:

$$\frac{ds^k}{dt} = -\beta k v s_{nq}^k, \tag{6}$$

$$\frac{di^k}{dt} = -\beta k v s^k_{nq} - \gamma i^k, \tag{7}$$

$$\frac{dr^k}{dt} = \gamma i^k. \tag{8}$$

$$v(t) = \Sigma_{k=0}^{\infty} q_k i^k_{nq}(t). \tag{9}$$

In this model, we have only two transitions: infection (from s to i) and recovery (from i to r). In the SIRCQ model, we have a few more transitions: infection (from s_{nq} to i_{nq}), recovery (from i_{nq} or i_q to r), quarantine from symptoms (from i_{nq} to i_q), contact tracing (from i_{nq} to i_q or from s_{nq} to s_q), and exit from quarantine (from s_q to s_{nq}). The compartments and the transitions are described in Fig. 1.

In the SIRCQ model the equations (6-9), are modified since the infection can occur only between non-quarantined vertices (s^k_{nq} and i^k_{nq}), Hence we obtain:

$$\frac{ds^k_{nq}}{dt} = -\beta k v s^k_{nq}, \tag{10}$$

$$\frac{di^k_{nq}}{dt} = -\beta k v s^k_{nq} - \gamma i^k_{nq}, \tag{11}$$

$$\frac{dr^k}{dt} = \gamma (i^k_{nq} + i^k_q). \tag{12}$$

$$v(t) = \Sigma_{k=0}^{\infty} q_k i^k_{nq}(t), \tag{13}$$

We now include the effect of symptoms. Symptoms occur only in infected people and only transfers people from I^k_{NQ} to I^k_Q. Therefore, equation (11) becomes:

$$\frac{di^k_{nq}}{dt} = -\beta k v s^k_{nq} - \gamma i^k_{nq} - p_{symptoms} i^k_{nq}, \tag{14}$$

and the new compartment satisfies:

$$\frac{di^k_q}{dt} = p_{symptoms} i^k_{nq} - \gamma i^k_q, \tag{15}$$

Finally, we address the transition probabilities of the contact tracing. Let us define p_{ct} as the rate of contact tracing, i.e. the rate of identifying contacts between quarantined people and others. This implies that the contact tracing results in transitions from S^k_{NQ} to S^k_Q and from I^k_{NQ} to I^k_Q. Hence it adds a positive term to S^k_Q, I^k_Q and a negative term to S^k_{NQ}, I^k_{NQ}. Note that

contacts with infected neighbors of any degree impact the contact tracing, and this results in a non-linear term that depends on $\hat{v}$ which is defined as the expected excess degree

$$\hat{v} = \Sigma_{k=0}^{\infty} q_k i_q^k(t). \tag{16}$$

Finally, we arrive at the equations of the model:

$$\frac{ds_{nq}^k}{dt} = -\beta k v s_{nq}^k - p_{ct} k \hat{v} s_{nq}^k + \theta_s s_q^k, \tag{17}$$

$$\frac{ds_q^k}{dt} = p_{ct} k \hat{v} s_{nq}^k - \theta_s s_q^k, \tag{18}$$

$$\frac{di_{nq}^k}{dt} = \beta k v s_{nq}^k - p_{ct} k \hat{v} i_{nq}^k - p_{symptoms} i_{nq}^k - \gamma i_{nq}^k, \tag{19}$$

$$\frac{di_q^k}{dt} = p_{ct} k \hat{v} i_{nq}^k + p_{symptoms} i_{nq}^k - \gamma i_q^k, \tag{20}$$

$$\frac{dr^k}{dt} = \gamma (i_{nq}^k + i_q^k). \tag{21}$$

k-regular graph case

Our system of equations (17-21) does not address the special case of k-regular graph which is in between the classical SIR model and the full arbitrary degree-distribution cases. This specific case is useful, when we know the average number of contacts per person, a parameter which can significantly improve the classical SIR model. In a k-regular graph all vertices have the same degree. Thus, the probability that a neighbor is infected and quarantined or infected and not quarantined is i_q and i_{nq}, respectively. In addition, instead of $5 \times K$ equations (where K is the number of different degrees of nodes), we now only have five equations. Thus, the equations become:

$$\frac{ds_{nq}}{dt} = -\beta k i_{nq} s_{nq} - p_{ct} k i_q s_{nq} + \theta_s s_q, \tag{22}$$

$$\frac{ds_q}{dt} = p_{ct} k i_q s_{nq} - \theta_s s_q, \tag{23}$$

$$\frac{di_{nq}}{dt} = \beta k i_{nq} s_{nq} - p_{ct} k i_q i_{nq} - p_{symptoms} i_{nq} - \gamma i_{nq}, \tag{24}$$

$$\frac{di_q}{dt} = p_{ct} k i_q i_{nq} + p_{symptoms} i_{nq} - \gamma i_q, \tag{25}$$

$$\frac{dr}{dt} = \gamma(i_{nq} + i_q). \tag{26}$$

We now show that for k-regular graphs, the system (22)-(26) can be reduced into a single equation, as follows:

Theorem 1. *Solving the system* (22)-(26) *is equivalent to solving the equation*

$$\frac{dm(i_q)}{dt} = -\beta k g(i_q) - p_{ct} k i_q m(i_q) + \theta_s f(i_q), \tag{27}$$

where:

$$m(i_q) = \frac{1}{\beta k} \frac{\frac{d^2 i_q}{dt^2} + \gamma \frac{di_q}{dt}}{\frac{di_q}{dt} + \gamma i_q} - \frac{p_{ct} \frac{di_q}{dt}}{\beta k p_{ct} i_q + \beta p_{symptoms}} + \frac{p_{symptoms}}{\beta k} + \frac{p_{ct} i_q}{\beta} + \frac{\gamma}{\beta k}, \tag{28}$$

$$f(i_q(t)) = e^{-\theta_s t} \int_0^t e^{\theta_s t} k p_{ct} i_q(t') m(t') dt', \tag{29}$$

$$g(i_q(t)) = i_0 e^{\int_0^t (\beta k m(t') - p_{symptoms} - k p_{ct} i_q(t') - \gamma) dt'}, \tag{30}$$

with the initial conditions: $s_{nq}(0) = 1 - i_0, i_{nq}(0) = i_0, i_q(0) = 0, s_q(0) = 0, r(0) = 0$. *All other compartments can be algebraically derived from* $i_q(t)$*:* $s_{nq}(t) = m(i_q(t))$, $s_q(t) = f(i_q(t))$, $s_{nq}(t) = g(i_q(t))$ *and* $r(t) = 1 - s_{nq}(t) - s_q(t) - i_{nq}(t) - i_q(t)$.

Note that (27) still needs to be solved numerically. However, solving a single differential equation is significantly simpler than solving a system of 5 non-linear differential equations.

Proof. To prove the theorem we can first solve the ODE (24) for i_{nq} with the initial condition $i_{nq}(0) = i_0$ obtaining:

$$i_{nq}(t) = i_0 e^{\int_0^t (\beta k s_{nq}(t') - p_{symptoms} - k p_{ct} i_q(t') - \gamma) dt'}. \tag{31}$$

We now substitute equation (31) with i_{nq} in equation (25). We do this in order to find a solution for s_{nq} so that $s_{nq} = f(i_q)$:

$$\frac{di_q}{dt} = (p_{symptoms} + k p_{ct} i_q) i_0 e^{\int_0^t (\beta k s_{nq} - p_{symptoms} - k p_{ct} i_q - \gamma) dt'} - \gamma i_q. \tag{32}$$

We isolate the exponent and use the natural logarithm on both sides:

$$\ln\left(\frac{\frac{di_q}{dt}+\gamma i_q}{(p_{symptoms}+kp_{ct}i_q)i_0}\right)=\int_0^t(\beta k s_{nq}-p_{symptoms}-kp_{ct}i_q-\gamma)dt'. \tag{33}$$

We now derive both sides and isolate s_{nq} to get:

$$s_{nq}(t)=\frac{1}{\beta k}\left(\frac{\frac{d^2i_q}{dt^2}+\gamma\frac{di_q}{dt}}{\frac{di_q}{dt}+\gamma i_q}-\frac{kp_{ct}\frac{di_q}{dt}}{kp_{ct}i_q+p_{symptoms}}+p_{symptoms}+kp_{ct}i_q+\gamma\right). \tag{34}$$

Afterward, we solve the ODE in equation (23) for s_q with the initial condition that $s_q(0)=0$:

$$s_q(t)=e^{-\theta_s t}\int_0^t e^{\theta_s t}kp_{ct}i_q(t')s_{nq}(t')dt'. \tag{35}$$

Since we can express s_{nq}, s_q, i_{nq} as functions of i_q, we can substitute equations (35, 34, 31) to equation (22) to get an ODE of i_q. In order to simplify the equation, we will use the following notations:

$$w(i_q(t))=\frac{\frac{d^2i_q(t)}{dt^2}+\gamma\frac{di_q(t)}{dt}}{\frac{di_q(t)}{dt}+\gamma i_q(t)}-\frac{kp_{ct}\frac{di_q(t)}{dt}}{kp_{ct}i_q(t)+p_{symptoms}}.$$

The ODE equation of i_q is:

$$\begin{aligned}\frac{1}{\beta k}\frac{dw(i_q(t))}{dt}+\frac{p_{ct}}{\beta}\frac{di_q(t)}{dt}=&-\left(i_0e^{\int_0^t w(i_q(t'))dt'}+\frac{p_{ct}i_q(t)}{\beta}\right)\left(w(i_q(t))+p_{symptoms}+kp_{ct}i_q(t)+\gamma\right)\\&+\theta_s e^{-\theta_s t}\int_0^t e^{\theta_s t'}\frac{p_{ct}}{\beta}i_q(t')\left(w(i_q(t'))+p_{symptoms}+kp_{ct}i_q(t')+\gamma\right)dt'.\end{aligned} \tag{36}$$

Once we solve the ODE of i_q numerically, we can calculate the rest of the compartments using equations (35, 34, 31). □

Calculation of the epidemic threshold with an arbitrary degree distribution

Theorem 2. *The epidemic threshold is* $R_0=\frac{\beta k_1}{p_{symptoms}+\gamma}$.

Proof. We use the next generation matrix method from [42] to calculate R_0.The infectious relevant compartments are i_{nq}^k and i_q^k. Their subsystem of equations is:

$$\frac{di_{nq}^k}{dt}=\beta k v s_{nq}^k-p_{ct}k\hat{v}i_{nq}^k-p_{symptoms}i_{nq}^k-\gamma i_{nq}^k, \tag{37}$$

$$\frac{di_q^k}{dt}=p_{ct}k\hat{v}i_{nq}^k+p_{symptoms}i_{nq}^k-\gamma i_q^k, \tag{38}$$

for $1 \leq k \leq n$, where $v(t) = \Sigma_{k=0}^{\infty} q_k i_{nq}^k(t)$ and $\hat{v}(t) = \Sigma_{k=0}^{\infty} q_k i_q^k(t)$.

The DFE (disease-free equilibrium) of our system of equations (17–21) is $\underbrace{\{e_1, e_1 \ldots, e_1\}}_{\text{K}}$, where K is the number of the degrees and $e_1 = (1, 0, 0, 0, 0)$. Meaning $s_{nq}^k = 1$, $s_q^k = i_{nq}^k = i_q^k = r^k = 0$ for all k.

We will first derive equations 37, 38 by $i_{nq}^{\tilde{k}}$ for each $1 \leq \tilde{k} \leq K$:

$$\frac{di_{nq}^k}{dt} = \beta q_{\tilde{k}} \tilde{k} s_{nq}^k - (p_{ct} \tilde{k} \hat{v} - p_{symptoms} - \gamma)\delta(\tilde{k} - k), \tag{39}$$

$$\frac{di_q^k}{dt} = (p_{ct} \tilde{k} \hat{v} + p_{symptoms})\delta(\tilde{k} - k), \tag{40}$$

where $\delta(\tilde{k} - k) = 1$ for $k = \tilde{k}$ and $\delta(\tilde{k} - k) = 0$ otherwise. Equations 39, 40 represent $2K$ equations for (2 for each $\tilde{k}$).

We will do the same derivation but by i_q^k this time:

$$\frac{di_{nq}^k}{dt} = -p_{ct} q_{\tilde{k}} \tilde{k} i_{nq}^k, \tag{41}$$

$$\frac{di_q^k}{dt} = p_{ct} q_{\tilde{k}} \tilde{k} i_{nq}^k - \gamma \delta(\tilde{k} - k). \tag{42}$$

Afterward, we will substitute the DFE and represent equations 39, 40, 41, 42 in a matrix form for all K degrees.

The $K \times 2K$ Jacobian matrix is represented as:

$$J = \begin{bmatrix} \frac{d}{di_{nq}^1}(\frac{di_{nq}^1}{dt})|_{DFE} & \cdots & \frac{d}{di_{nq}^K}(\frac{di_{nq}^1}{dt})|_{DFE} & \frac{d}{di_q^1}(\frac{di_{nq}^1}{dt})|_{DFE} & \cdots & \frac{d}{di_q^K}(\frac{di_{nq}^1}{dt})|_{DFE} \\ \vdots & \ddots & \vdots & \vdots & \ddots & \vdots \\ \frac{d}{di_{nq}^1}(\frac{di_{nq}^K}{dt})|_{DFE} & \cdots & \frac{d}{di_{nq}^K}(\frac{di_{nq}^K}{dt})|_{DFE} & \frac{d}{di_q^1}(\frac{di_{nq}^K}{dt})|_{DFE} & \cdots & \frac{d}{di_q^K}(\frac{di_{nq}^K}{dt})|_{DFE} \end{bmatrix}. \tag{43}$$

If we compute J we get:

$$J = \begin{bmatrix} A - (p_{symptoms} + \gamma)I & O \\ p_{symptoms} I & -\gamma I \end{bmatrix}, \tag{44}$$

where *I* and *O* are the identity and zero matrix of order K, respectively, and the matrix A is:

$$A = \begin{bmatrix} \beta q_1 & \cdots & \beta q_K \\ \vdots & \ddots & \vdots \\ K\beta q_1 & \cdots & n\beta q_K \end{bmatrix}. \tag{45}$$

The Jacobian matrix is decomposed into a transmission matrix F and transition matrix V:

$$F = \begin{bmatrix} A & O \\ O & O \end{bmatrix} \tag{46}$$

$$V = \begin{bmatrix} (p_{symptoms} + \gamma)I & O \\ -p_{symptoms}I & \gamma I \end{bmatrix}. \tag{47}$$

The inverse of the transition matrix is:

$$V^{-1} = \begin{bmatrix} \frac{1}{p_{symptoms}+\gamma} I & O \\ \frac{p_{symptoms}}{p_{symptoms}+\gamma} I & \frac{1}{\gamma} I \end{bmatrix}.$$

Next, we find the spectral radius of the next generation matrix FV^{-1}:

$$\rho(FV^{-1}) = \rho\left(\frac{1}{p_{symptoms} + \gamma} A\right) = \frac{1}{p_{symptoms} + \gamma}\rho(A).$$

Using Lemma 3 we obtain:

$$R_0 = \rho(FV^{-1}) = \frac{\beta}{p_{symptoms} + \gamma}\Sigma_{k=1}^{K} k q_k.$$

Finally, we get:

$$R_0 = \frac{\beta k_1}{p_{symptoms} + \gamma}, \tag{48}$$

where k_1 is the mean excess degree. □

Lemma 3. *The spectral radius of A is $\Sigma_{k=1}^{n} k q_k$.*

Proof. Let the vectors $\mathbf{a}, \mathbf{b}$ be defined by:

$$\mathbf{a} = \begin{pmatrix} 1 \\ 2 \\ \vdots \\ K \end{pmatrix}, \mathbf{b} = \begin{pmatrix} \beta q_1 \\ \beta q_2 \\ \vdots \\ \beta q_K \end{pmatrix}.$$

We can clearly see that $A = \mathbf{a}\mathbf{b}^T$. The matrix A has rank 1 since all the rows of A's are linearly dependent. Hence there is a single positive eigenvalue which is $\mathbf{a}$ since

$$A\mathbf{a} = (\mathbf{a}\mathbf{b}^T)\mathbf{a} = \mathbf{a}(\mathbf{b}^T\mathbf{a}) = \lambda\mathbf{a}, \tag{49}$$

where $\lambda = \Sigma_{k=1}^{K} k\beta q_k$ is the positive eigenvalue. Because A has only a single non-zero eigenvalue, λ is also the maximal eigenvalue and thus the spectral radius. □

Calculation of the epidemic threshold for k-regular graph. In the k-regular case the epidemic threshold can be derived in a simpler more intuitive way by considering equation (24). An epidemic is spreading only when the factor $\beta k s_{nq} - p_{symptoms} - k p_{ct} i_q - \gamma$ is positive. In early phase of the epidemic $s_{nq} \approx 1$ and $i_q \approx 0$, therefore, equation (24) becomes:

$$\frac{di_{nq}}{dt} = (\beta k - p_{symptoms} - \gamma) i_{nq} > 0. \tag{50}$$

Thus an outbreak occurs when

$$R_0 = \frac{\beta k}{p_{symptoms} + \gamma} > 1. \tag{51}$$

We can also use the next-generation matrix method to get the same result, where the regular graph case is easier than the general degree distribution.

Numerical solution of the equations

In order to solve the differential equations numerically, we used the explicit Runge-Kutta method of order 5(4) [44] as our integration method. We used a single vector of all compartments for the calculation, i.e.:

$$\{s_{nq}^1, s_{nq}^2 \ldots, s_{nq}^K, s_q^1, s_q^2 \ldots, s_q^K, i_{nq}^1, i_{nq}^2 \ldots, i_{nq}^K, i_q^1, i_q^2 \ldots, i_q^K, r^1, r^2 \ldots, r^K\}$$

with the initial conditions:

$$\forall k : s_{nq}^k = s_{nq}(0), s_q^k = s_q(0), i_{nq}^k = i_{nq}(0), i_q^k = i_q(0), r^k = r(0)$$

The initial conditions stay the same for each degree to get the correct initial condition for the corresponding compartment. For example, for susceptible and not quarantined:

$$s_{nq}(t=0) = \Sigma_k p_k s_{nq}(0) = s_{nq}(0) \Sigma_k p_k = s_{nq}(0)$$

Agent-based model

In order to verify the model, we developed simulations of an agent-based model. The simulation results are then compared to the predicted results of the SIRCQ model.

Population network: In our simulations, we use a population of $n = 10^5$ and a configuration

model to attach the proper degree distribution to the vertices upon each realization. We used random graphs with a power law degree distribution as well as regular graphs with varying degrees. The reasoning for using a power-law degree distribution is that many real networks, such as contact networks, have been shown to exhibit scale-free properties as mentioned in [45]. Regular graphs are special cases with a single degree. This model generalizes the classical SIR, where each node has only a relatively small number of possible contacts.

The probability $P(k)$ that a node is connected to k other nodes follows a Power-law:

$$P(k) \sim k^{-\alpha} \tag{52}$$

where α is usually ranging between $2 \leq \alpha \leq 3$. We used the following parameters:

α	Degree Range
2	[8, 1506]

We chose a small α and the degree range to have a slower and more realistic fade of degrees.

Epidemic parameters: The parameters we chose for the epidemic unless noted otherwise are

γ	$p_{symptoms}$	θ_s
0.14	0.25	0.07

The reason we chose these parameters is to have a mean time of recovery of 7 days, mean time of symptoms appearance of 4 days and quarantine time of 14 days. Because the rates of $\gamma, p_{symptoms}, \theta_s$ act like a geometric distribution, the rates need to be *1/(mean time)*.

References

[1] Clemente-Suárez, V. J. *et al.* The impact of the covid-19 pandemic on social, health, and economy. *Sustainability* **13** (2021).

[2] Liu, W. *et al.* Modelling the emerging covid-19 epidemic and estimating intervention effectiveness—taiwan, china, 2021. *China CDC weekly* **3**, 716 (2021).

[3] Cauchemez, S., Valleron, A.-J., Boelle, P.-Y., Flahault, A. & Ferguson, N. M. Estimating the impact of school closure on influenza transmission from sentinel data. *Nature* **452**, 750–754 (2008).

[4] Anderson, R. M., Heesterbeek, H., Klinkenberg, D. & Hollingsworth, T. D. How will country-based mitigation measures influence the course of the COVID-19 epidemic? *The lancet* **395**, 931–934 (2020).

[5] Hollingsworth, T. D., Klinkenberg, D., Heesterbeek, H. & Anderson, R. M. Mitigation strategies for pandemic influenza A: balancing conflicting policy objectives. *PLoS computational biology* **7**, e1001076 (2011).

[6] Diekmann, O., Heesterbeek, H. & Britton, T. *Mathematical Tools for Understanding Infectious Disease Dynamics*, vol. 7 ((Princeton University Press, Princeton, 2013)).

[7] Brauer, F., Castillo-Chavez, C. & Feng, Z. *Mathematical Models in Epidemiology*, vol. 32 ((Springer, Berlin, 2019)).

[8] Bissett, K. R., Cadena, J., Khan, M. & Kuhlman, C. J. Agent-based computational epidemiological modeling. *Journal of the Indian Institute of Science* 1–25 (2021).

[9] Marshall, B. D. & Galea, S. Formalizing the Role of Agent-Based Modeling in Causal Inference and Epidemiology. *American Journal of Epidemiology* **181**, 92–99 (2014).

[10] Blackwood, J. C. & Childs, L. M. An introduction to compartmental modeling for the budding infectious disease modeler. *Letters in Biomathematics* **5**, 195–221 (2018).

[11] Brauer, F., Van den Driessche, P., Wu, J. & Allen, L. J. *Mathematical Epidemiology*, vol. 1945 (Springer, 2008).

[12] Newman, M. *Networks* ((Oxford University Press, Oxford, 2018)).

[13] Bonabeau, E. Agent-based modeling: Methods and techniques for simulating human systems. *Proceedings of the national academy of sciences* **99**, 7280–7287 (2002).

[14] Tolles, J. & Luong, T. Modeling epidemics With compartmental models. *JAMA* **323**, 2515–2516 (2020).

[15] Andersson, P. & Lindenstrand, D. A stochastic SIS epidemic with demography: initial stages and time to extinction. *Journal of mathematical biology* **62**, 333–348 (2011).

[16] Hethcote, H., Zhien, M. & Shengbing, L. Effects of quarantine in six endemic models for infectious diseases. *Mathematical biosciences* **180**, 141–160 (2002).

[17] Ferrari, M. J., Perkins, S. E., Pomeroy, L. W. & Bjørnstad, O. N. Pathogens, social networks, and the paradox of transmission scaling. *Interdisciplinary perspectives on infectious diseases* **2011** (2011).

[18] Newman, M. E. Spread of epidemic disease on networks. *Physical review E* **66**, 016128 (2002).

[19] Meyers, L. A., Pourbohloul, B., Newman, M. E., Skowronski, D. M. & Brunham, R. C. Network theory and sars: predicting outbreak diversity. *Journal of theoretical biology* **232**, 71–81 (2005).

[20] Volz, E. SIR dynamics in random networks with heterogeneous connectivity. *Journal of mathematical biology* **56**, 293–310 (2008).

[21] Miller, J. C. A note on a paper by Erik Volz: SIR dynamics in random networks. *Journal of mathematical biology* **62**, 349–358 (2011).

[22] Li, J., Wang, J. & Jin, Z. SIR dynamics in random networks with communities. *Journal of Mathematical Biology* **77**, 1117–1151 (2018).

[23] Cohen, K. & Leshem, A. Suppressing the impact of the COVID-19 pandemic using controlled testing and isolation. *Scientific Reports* **11**, 6279 (2021).

[24] Ng, Y. & others. Evaluation of the Effectiveness of Surveillance and Containment Measures for the First 100 Patients with COVID-19 in Singapore — January 2–February 29, 2020. *Morbidity and mortality weekly report* **69**, 307 (2020).

[25] Mbunge, E. Integrating emerging technologies into COVID-19 contact tracing: Opportunities, challenges and pitfalls. *Diabetes & Metabolic Syndrome: Clinical Research & Reviews* **14**, 1631–1636 (2020).

[26] Memon, Z., Qureshi, S. & Memon, B. R. Assessing the role of quarantine and isolation as control strategies for covid-19 outbreak: a case study. *Chaos, Solitons & Fractals* **144**, 110655 (2021).

[27] Hellewell, J. *et al.* Feasibility of controlling COVID-19 outbreaks by isolation of cases and contacts. *The Lancet Global Health* **8**, e488–e496 (2020).

[28] Schiffer, A.-M. Controlling COVID-19. *Nature Human Behaviour* **4**, 450–450 (2020).

[29] Hernández-Orallo, E., Manzoni, P., Calafate, C. T. & Cano, J.-C. Evaluating how smartphone contact tracing technology can reduce the spread of infectious diseases: The case of COVID-19. *Ieee Access* **8**, 99083–99097 (2020).

[30] Kryven, I. & Stegehuis, C. Contact tracing in configuration models. *Journal of Physics: Complexity* **2**, 025004 (2021).

[31] Aleta, A. *et al.* Modelling the impact of testing, contact tracing and household quarantine on second waves of COVID-19. *Nature Human Behaviour* **4**, 964–971 (2020).

[32] Sturniolo, S., Waites, W., Colbourn, T., Manheim, D. & Panovska-Griffiths, J. Testing, tracing and isolation in compartmental models. *PLoS computational biology* **17**, e1008633 (2021).

[33] Chiu, W. A., Fischer, R. & Ndeffo-Mbah, M. L. State-level needs for social distancing and contact tracing to contain COVID-19 in the United States. *Nature Human Behaviour* **4**, 1080–1090 (2020).

[34] Lee, D.-S., Liu, T.-Z., Zhang, R. & Chang, C.-S. A Degree Based Approximation of an SIR Model with Contact Tracing and Isolation. *Preprint at* `https://arxiv.org/abs/2212.09093` (2022).

[35] James, A. *et al.* Successful contact tracing systems for COVID-19 rely on effective quarantine and isolation. *PLoS One* **16**, e0252499 (2021).

[36] Ferretti, L. *et al.* Quantifying SARS-COV-2 transmission suggests epidemic control with digital contact tracing. *science* **368**, eabb6936 (2020).

[37] Ienca, M. & Vayena, E. On the responsible use of digital data to tackle the covid-19 pandemic. *Nature medicine* **26**, 463–464 (2020).

[38] Sun, K. & Viboud, C. Impact of contact tracing on SARS-COV-2 transmission. *The Lancet Infectious Diseases* **20**, 876–877 (2020).

[39] World Health Organization. Contact tracing and quarantine in the context of covid-19: interim guidance, 6 july 2022 (2022).

[40] Gilbert, E. N. Random graphs. *The Annals of Mathematical Statistics* **30**, 1141–1144 (1959).

[41] Erdős, P. & Rényi, A. On random graphs I. *Publ. math. debrecen* **6**, 18 (1958).

[42] Van den Driessche, P. & Watmough, J. Reproduction numbers and sub-threshold endemic equilibria for compartmental models of disease transmission. *Mathematical biosciences* **180**, 29–48 (2002).

[43] Moreno, Y., Pastor-Satorras, R. & Vespignani, A. Epidemic outbreaks in complex heterogeneous networks. *The European Physical Journal B-Condensed Matter and Complex Systems* **26**, 521–529 (2002).

[44] Dormand, J. R. & Prince, P. J. A family of embedded Runge-Kutta formulae. *Journal of computational and applied mathematics* **6**, 19–26 (1980).

[45] Barabási, A.-L. & Albert, R. Emergence of scaling in random networks. *Science* **286**, 509–512 (1999).